

Selectivity of direct and network-mediated stimulation of the retinal ganglion cells with epi-, sub- and intraretinal electrodes

David Boinagrov^{1,2}, Susanne Pangratz-Fuehrer^{1,3}, Georges Goetz^{1,4}
and Daniel Palanker^{1,3}

¹ Hansen Experimental Physics Laboratory, Stanford University, Stanford, CA 94305, USA

² Department of Physics, Stanford University, Stanford, CA 94305, USA

³ Department of Ophthalmology, Stanford University, Stanford, CA 94305, USA

⁴ Department of Electrical Engineering, Stanford University, Stanford, CA 94305, USA

E-mail: boinagrov@gmail.com

Received 13 July 2013, revised 24 December 2013


Accepted for publication 21 January 2014

Published 10 March 2014

Abstract

Objective. Intra-retinal placement of stimulating electrodes can provide close and stable proximity to target neurons. We assessed improvement in stimulation thresholds and selectivity of the direct and network-mediated retinal stimulation with intraretinal electrodes, compared to epiretinal and subretinal placements. **Approach.** Stimulation thresholds of the retinal ganglion cells (RGCs) in wild-type rat retina were measured using the patch-clamp technique. Direct and network-mediated responses were discriminated using various synaptic blockers. **Main results.** Three types of RGC responses were identified: short latency (SL, $\tau < 5$ ms) originating in RGCs, medium latency (ML, $3 < \tau < 70$ ms) originating in the inner nuclear layer and long latency (LL, $\tau > 40$ ms) originating in photoreceptors. Cathodic epiretinal stimulation exhibited the lowest threshold for direct RGC response and the highest direct selectivity (network/direct thresholds ratio), exceeding a factor of 3 with pulse durations below 0.5 ms. For network-mediated stimulation, the lowest threshold was obtained with anodic pulses in OPL position, and its network selectivity (direct/network thresholds ratio) increased with pulse duration, exceeding a factor of 4 at 10 ms. Latency of all three types of responses decreased with increasing strength of the stimulus. **Significance.** These results define the optimal range of pulse durations, pulse polarities and electrode placement for the retinal prostheses aiming at direct or network-mediated stimulation of RGCs.

Keywords: epiretinal, subretinal, intraretinal stimulation, retinal prostheses, stimulation selectivity

 Online supplementary data available from stacks.iop.org/JNE/11/026008/mmedia

(Some figures may appear in colour only in the online journal)

Introduction

Retinal degenerative diseases, such as age-related macular degeneration and retinitis pigmentosa, lead to blindness due to the loss of photoreceptors (Ferris *et al* 1984, Phelan and Bok 2000, Daiger *et al* 2007). However, a significant number of the inner retinal neurons survive in such diseases

(Stone *et al* 1992, Kim *et al* 2002, Mazzoni *et al* 2008), raising the possibility of a functional restoration of vision by stimulation of the remaining inner retinal neurons. Multiple approaches to restoration of sight in individuals affected by these diseases are being explored, including optogenetics (Busskamp and Roska 2011, Reutsky-Gefen *et al* 2013), molecular photoswitches (Polosukhina *et al* 2012), stem

cells-based therapy (Schraermeyer *et al* 2001, Enzmann *et al* 2009) and electronic retinal prostheses (Rizzo *et al* 2001, Zrenner 2002, Weiland *et al* 2005, Palanker *et al* 2005, Klauke *et al* 2011, Fujikado *et al* 2011, Hadjinicolaou *et al* 2012). Recent clinical trials of epiretinal electronic implants (Humayun *et al* 2011, da Cruz *et al* 2013) in patients blinded by retinitis pigmentosa demonstrated equivalent visual acuity up to 20/1260 in the most successful patient, leading to clinical approval in US and Europe. Even better visual acuity of 20/550 has been recently demonstrated with subretinal implant (Stingl *et al* 2013).

The epiretinal approach to retinal prosthetics aims at direct stimulation of the retinal ganglion cells (RGCs) using electrodes placed on the inner limiting membrane of the retina. Encoding visual information by direct activation of RGCs implies that each stimulation pulse produces a single action potential (AP) with a latency of about 1 ms (Sekirnjak *et al* 2006, Boinagrov *et al* 2010, Eickenscheidt *et al* 2012). On the contrary, stimulation of the inner retinal neurons in many cases results in the generation of bursts of spikes (Stett *et al* 2000, Tsai *et al* 2009), resembling ON retinal response to a short pulse of light. Epiretinal stimulation can evoke both, the early (direct) responses (~ 1 ms) and late (network-mediated) responses. The network-mediated origin of the latter was proven by inhibiting neurotransmitter release with cadmium or postsynaptic glutamate receptor antagonists (Stett *et al* 2000, Margalit and Thoreson 2006). RGCs can accurately follow electrical stimulation with rates up to 250 Hz, which corresponds to the maximum spike frequencies in the natural light responses (Fried *et al* 2006). Therefore, direct RGC stimulation may allow precise mimicking of RGC bursts characteristic to normal vision (Sekirnjak *et al* 2006, Hottowy *et al* 2012), so long as the network response is avoided. Such strategy requires (a) knowledge of the retinal code for each RGC type, (b) identification of each cell type, and (c) accessibility of each RGC to selective stimulation with a proper sequence of pulses. However, (a) the retinal code is not yet well understood, (b) it is not clear how to identify various RGC types in degenerate retina, especially *in-vivo*, and (c) not every cell in the multilayered ganglion cell layer (GCL) can be selectively approached and stimulated. Moreover, as epiretinal electrodes are positioned on top of the nerve fiber layer and axonal stimulation thresholds are similar to that of RGC somas, axonal stimulation is hard to avoid. It is likely the cause of arcuate or wedged visual percepts in patients stimulated with single epiretinal electrodes (Nanduri *et al* 2012).

An alternative approach is to stimulate the first layer of neurons after photoreceptors—the inner nuclear layer (INL), and rely on the retinal network conversion of single pulse stimuli into RGC bursting (Mathieson *et al* 2012, Mandel *et al* 2013). Retinal reorganization associated with degeneration though will likely alter the normal network responses to subretinal stimulation (Jones and Marc 2005), potentially limiting the benefits of engaging the retinal circuitry. Both types of stimulation result in retinal signals very different from the natural retinal code, so both strategies rely on brain's ability to learn the new signaling code over time, as it happens with the cochlear implants. Both approaches produced very

encouraging results in clinical trials, and subretinal approach yielded the most encouraging results with the best visual acuity of 20/550 in the most successful patient (Stingl *et al* 2013).

It remains unclear though to what extent the direct and network-mediated responses are involved in epi- and subretinal stimulation with various pulse parameters. In this paper we describe two types of selectivity of the RGC stimulation—direct and network-mediated. Direct selectivity defines a dynamic range over which a direct response of RGCs can be elicited without activation of the inner retinal network. It is defined as a ratio of the thresholds of the network-mediated and direct responses. Network selectivity quantifies the opposite effect: the ability of eliciting a network-mediated response without direct activation of RGCs. It is defined as a ratio of the stimulation thresholds of direct and network-mediated responses for a given stimulus duration, polarity and electrode location. In the present study we examined direct and network selectivities of RGC stimulation as a function of the stimulus polarity, pulse width and electrode location in the rat retina.

To achieve closer proximity to the target neurons in subretinal approach three-dimensional implants with either chamber arrays (Palanker *et al* 2004, Palanker *et al* 2005, Butterwick *et al* 2009), pillar arrays (Loudin *et al* 2007, Mathieson *et al* 2012) or other 3D shapes (Khraiche *et al* 2011, Bendali *et al* 2012) have been proposed. In such arrangements, the electrodes can be placed in the middle of the retina, close to the INL. Similarly, penetrating electrodes have also been proposed for epiretinal approach (Ganesan *et al* 2010, Gefen 2012). To assess potential advantages of intraretinal electrodes, we compared the thresholds and selectivity of direct and network-mediated stimulation with electrodes placed inside the retina (just above and just below the INL) to the thresholds measured in epiretinal and subretinal positions.

Materials and methods

Retinal preparation

Male wild-type Long-Evans rat (Charles River Laboratories International, Inc., Wilmington, MA) retinas were used for these experiments. Rats were handled humanely, according to the guidelines of the Association for Research in Vision and Ophthalmology (ARVO) and protocols approved by the Institutional Animal Care and Use Committee at Stanford Medical School. P45–P80 animals were anesthetized by inhalation of evaporated isoflurane (1 g l^{-1} , Baxter Healthcare Corporation, Deerfield, IL) and subsequently euthanized with an intraperitoneal injection of Beuthanasia-D (1 ml kg^{-1} of animal weight, Schering-Plough Animal Health Corp., Union, NJ). The eyes were enucleated and hemisected in the Ames medium (Sigma-Aldrich, St. Louis, MO) bubbled with a mixture of 95% O_2 and 5% CO_2 (Airgas, Redwood City, CA). After hemisecting the eye, lens and vitreous humor were removed, and the retina was detached from the pigment epithelium. Subsequently, retina was cut into pieces $\sim 2 \text{ mm}^2$ in size, attached to filter paper, and kept at room temperature under ambient light conditions before being placed in the perfusion chamber photoreceptor side

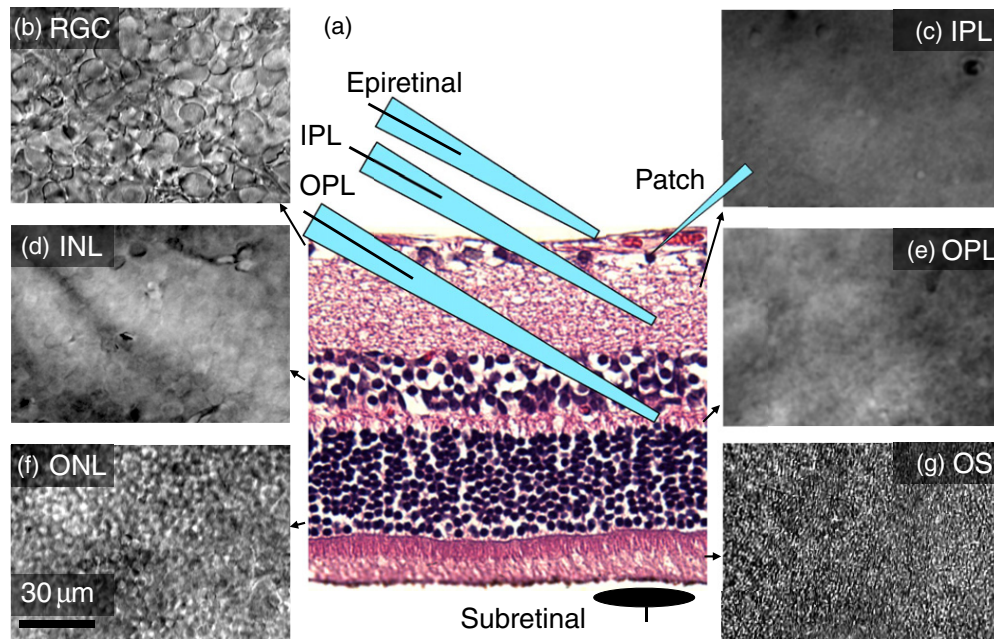


Figure 1. Long-Evans rat retina. (a) Retinal histology illustrating positioning of the patch pipette, and four positions of the stimulation electrodes: epiretinal, IPL, OPL and subretinal. (b)–(g) Appearance of the retinal layers in the DIC microscope: (b) RGC, (c) inner plexiform (IPL), (d) inner nuclear (INL), (e) outer plexiform (OPL), (f) outer nuclear (ONL), (g) photoreceptors outer segments (OS).

down (see figure 1). A hole (~ 1 mm in diameter) was cut in the center of the filter paper to allow imaging of the RGCs via differential interference contrast (DIC) microscope in transmitted illumination. Artificial cerebrospinal fluid (ACSF, containing in mM: NaCl 126, glucose 10, KCl 2.5, $\text{NaH}_2\text{PO}_4 \cdot \text{H}_2\text{O}$ 1.25, $\text{MgSO}_4 \cdot 7\text{H}_2\text{O}$ 1, $\text{CaCl}_2 \cdot 2\text{H}_2\text{O}$ 2, NaHCO_3 26), bubbled with 95% O_2 and 5% CO_2 (pH 7.3) was heated via inline heater and delivered to the perfusion chamber (bath) at a rate of ~ 3 ml min^{-1} to maintain the bath temperature at 31 ± 1 °C. In pharmacological experiments, synaptic blockers were applied to the ACSF.

Recording from RGCs

Cells were classified as ganglion based on their location in the ganglion cell layer and presence of prominent fast inward sodium currents, although occasional occurrence of some displaced amacrine cells cannot be completely excluded (Jeon *et al* 1998). The patch-clamp technique (Sakmann and Neher 1984) was used to record the cell potential of individual RGCs with soma diameters larger than average (> 15 μm). Micropipettes with tips of ~ 1 μm outer diameter and resistance values of 5–15 MΩ were pulled from borosilicate glass tubes using a Sutter P-2000 pipette puller (Sutter Instrument Co., Novato, CA). The pipette electrolyte solution contained: 116 mM KCH_3SO_4 ; 10 mM KCl, 10 mM HEPES; 1 mM CaCl_2 ; 0.5 mM EGTA; 4 mM $\text{Mg}_2\text{-ATP}$; 0.5 mM $\text{Na}_2\text{-GTP}$ (pH 7.3; 270 mOsm osmolarity, all from Sigma-Aldrich, St Louis, MO). A silver-chloride electrode was immersed in the patch pipette, and a large silver wire placed in the perfusion chamber served as a reference electrode. Signal recording in the current clamp mode was performed with a Multiclamp 700A Amplifier (Molecular Devices, Sunnyvale, CA), digitized with a Digidata 1440 (Molecular Devices), and

recorded on a PC with PClamp 10.2 Software (Molecular Devices). The health of recorded RGC was verified by assuring that its resting potential was in the range of -70 ± 10 mV, that it did not shift by more than 10 mV during the course of recordings, and that the amplitude of AP did not decrease by more than half of its initial value.

Retinal stimulation

Stimulation was performed with electrodes placed in four different positions in the retina: epiretinal, two intraretinal (in IPL and OPL) and subretinal (see figure 1). For epiretinal and intraretinal stimulation, electrical current was delivered by a micropipette of 4–8 μm diameter, filled with ACSF and containing an immersed thick silver or platinum wire electrode. An epiretinal pipette was placed 10–20 μm away from the recorded RGC, without penetrating the nerve fiber layer. The intraretinal stimulation pipettes were placed under the recorded RGCs, with a lateral displacement within 20–40 μm. Vertical positioning of the stimulating pipette at proper depth was controlled by focusing the microscope on individual retinal layers (figure 1). Typically, for IPL placement the pipette tips were immersed at a depth of 20–30 μm, while for OPL—at 70–80 μm. Subretinal stimulation electrode was a 40 μm disc coated with sputtered iridium oxide film (SIROF), and wired by an insulated lead deposited on a glass base placed under the retina. A large electrode placed in the bath far away from the active electrode was used as a return. Rectangular monophasic cathodic and anodic pulses of 0.1–100 ms in duration were generated with an isolated pulse stimulator, Model 2100 (A-M Systems, Carlsborg, WA) and delivered at a repetition rate of 1 Hz. Latency of an elicited AP was defined as a time interval between the stimulus onset and the peak voltage of the AP. 20 consecutive pulses were delivered for any given

current and duration to calculate the probability of eliciting a response. Stimulation threshold was defined as a setting corresponding to a 50% probability of eliciting AP. The charge in monophasic waveform was balanced by a low-amplitude long discharge between consecutive pulses. The strength–duration (S–D) relationship of direct and network-mediated stimulation thresholds was determined for each location.

Data analysis

Stimulation thresholds were measured for each stimulation configuration (duration, polarity, electrode location) and response type (short, medium, and long latency: SL, ML, LL). Thresholds varied from cell to cell, and for the purpose of statistical analysis they were assumed to be distributed log-normally. Thus, an estimate for the mean threshold value was calculated as a geometric mean of individual thresholds, and the estimate for the error of mean was done using the geometric standard deviation. According to the log-normal statistics, 70% of the data lie within the estimated error of the mean value. Statistical significance of hypotheses were verified using two-tailed two-sample Student's *t*-test, assuming unequal variances.

RGC classification

The type of the RGC (ON versus OFF) was determined by extending the method described in Margolis *et al* (2010) to RGCs in our experiment. We injected hyperpolarizing intracellular current, which exhibited a characteristic rebound spike selectively in OFF RGCs. Intracellular injection of a long anodic pulse performed with the patch pipette resulted in immediate spiking (figure 2). Cathodic current suppressed any spiking during the pulse, but elicited the rebound spike in OFF RGCs, but not in ON cells. This rebound spiking is attributed to inactivating voltage sensitive calcium ion-channels in the RGC dendrites, which are absent in ON RGCs (Margolis *et al* 2010). To validate the Margolis classification, the RGC responses to green light stimuli have been recorded in a subset of cells ($n = 6$) using 200 ms pulses of 2 nW mm^{-2} . Rebound spike to hyperpolarizing current has been observed only in cells which decreased their spiking rate under light (OFF response), while in the cells exhibiting increase in the spiking rate upon illumination (ON response), the rebound spike was absent, confirming applicability of Margolis test to large RGCs in the rat retina. Since Margolis' classification was not established for all RGC subtypes, it can be considered a tentative one.

Results

Three types of responses

Time-locked RGC responses with latency in the 0.5–400 ms range were classified in three groups—SL, ML and LL. Some cells exhibited all three types of response (figure 3(a)), while others had just two (figures 4(a)–(c)) or one type, depending on electrode location, stimulus strength, duration and polarity. Addition of pharmacological agents was used to classify the responses. ML and LL responses disappeared upon addition

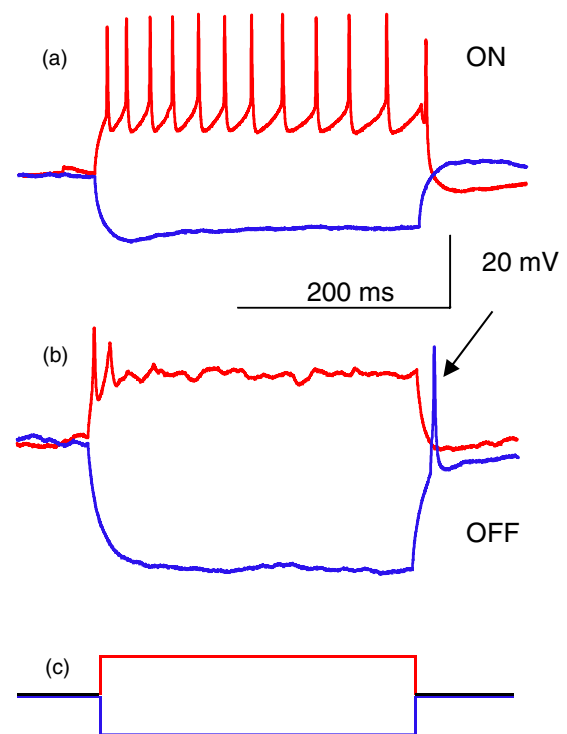


Figure 2. Response of RGCs to intracellular stimulation. (a) +100 pA current injected into ON cell for 300 ms elicits spiking during the pulse (red), while −100 pA current results in no spiking during and after the pulse (blue). (b) Injection of +100 pA of current into the OFF cell results in initial spiking (red), while −100 pA of current produces a rebound spike after the end of stimulus (blue, indicated by the arrow). (c) Cathodic (blue) and anodic (red) intracellular pulses injected.

of $100 \mu\text{M}$ of CdCl_2 , which blocks synaptic transmission (Sekirnjak *et al* 2006, Tsai *et al* 2009), while SL responses remained (figure 4). This confirms that SL responses are elicited directly in RGCs, while ML and LL originate in the retinal network and are transmitted to RGCs via synaptic connections.

LL responses in ON RGCs ($N = 7$) disappeared upon addition of $100 \mu\text{M}$ of L-AP4, even with stimuli stronger than the original threshold, while ML and SL responses remained (figure 3). Since L-AP4 blocks the metabotropic receptors (Pin and Duvoisin 1995) in synapses connecting photoreceptors to ON bipolar cells, disappearance of the LL spiking and preservation of ML firing is likely to indicate that LL responses originate in photoreceptors, while ML stimulation originates in the inner retinal neurons (bipolar, horizontal or amacrine cells). However, one cannot completely exclude a possibility that LL responses arise from the lateral spread of the electrical stimulation via horizontal and amacrine cells, which might also be affected by the L-AP4 blocker, either directly or via ON bipolar cells.

Latency of each type of response (SL, ML and LL) was measured as a function of the stimulus amplitude for 30 cells with little spontaneous activity, using stimulus durations of 0.5–4 ms for SL response and 0.2–10 ms for ML and LL responses. Figure 5 shows the minimum latency as a function of the ratio of the pulse amplitude to stimulation threshold,

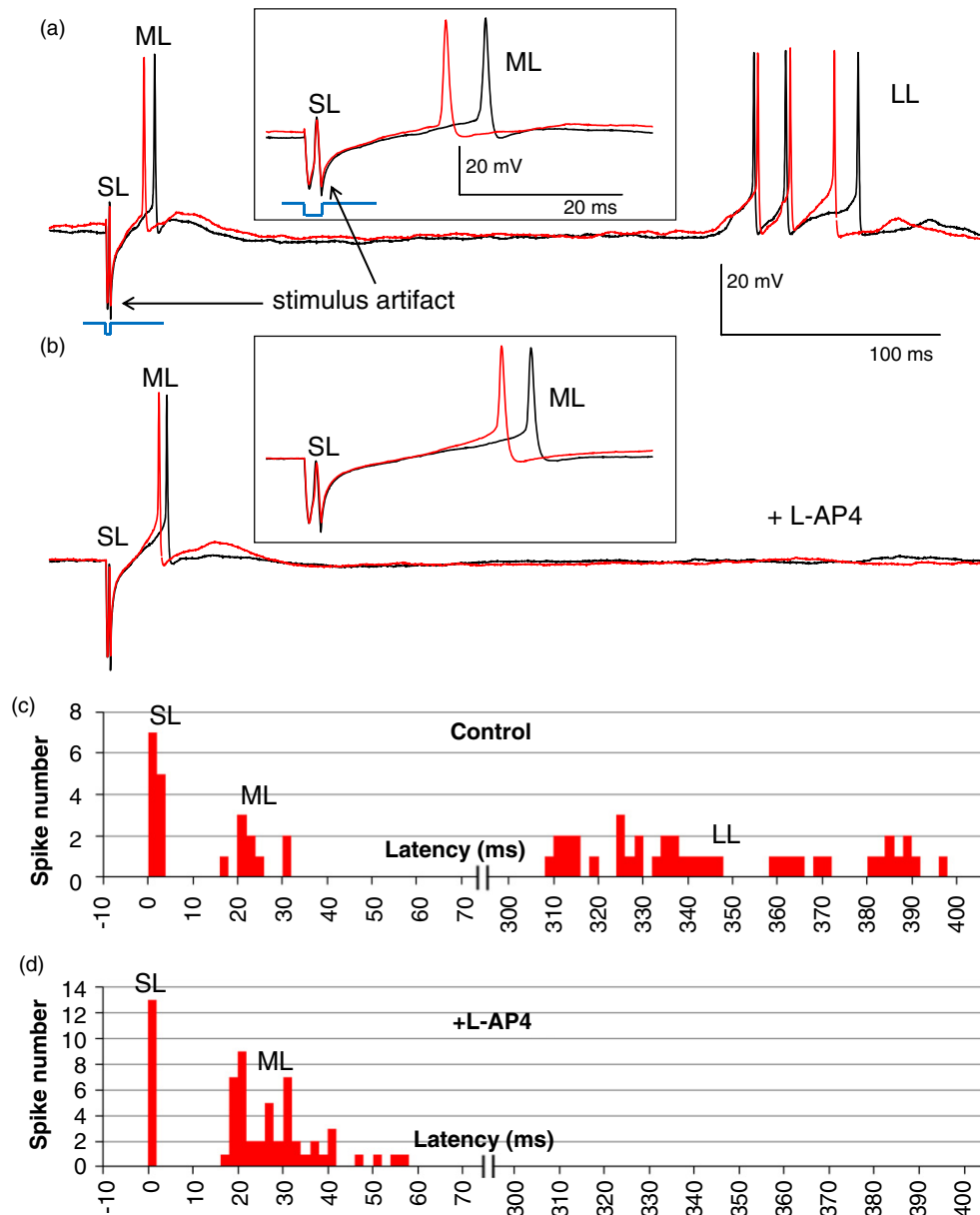


Figure 3. Traces illustrating three types of RGC responses to 2 ms, 10 μ A cathodic stimuli with electrode located in OPL. (a) Two control traces including the stimulation artifact and the SL, ML and LL responses. (b) Two traces with L-AP4 blocker, demonstrating the SL and ML spiking, but no LL response. The insets show magnified view of the SL and ML responses. Stimulating pulses are shown in blue, and scale bars are the same for (a) and (b). (c) and (d) PSTH for 20 traces before (c) and after (d) L-AP4 application, with stimulus applied at 0 ms. No events were detected in the cut-out section of 70–300 ms.

measured in 20 trials per cell for each stimulus settings. In cases of a burst response, latency of the first spike in the train was considered. For each cell, the data were then fitted with a power function and these fits were averaged for each type of response. In figure 5, the average fit for each type of response is plotted as a solid line with the corresponding standard deviation shown as a shaded area. Since latencies could not be measured with high precision below 1 ms (especially for high stimulus strength), the trend line for direct response (SL) extrapolated below 1 ms is shown in dash. For all types of response the latencies decreased with increasing stimulus strength.

Strength–duration relationship of the stimulation threshold

Stimulation thresholds strongly varied with pulse polarities, electrode location and type of the response, but the shape of the S–D relationship for each type of response was independent of pulse polarity and electrode location. Thresholds were measured as a function of pulse duration for all three types of responses: direct (SL, $N = 17$) and two types of network-mediated responses—ML ($N = 14$) and LL ($N = 7$). For averaging, the S–D relationship curve for each cell and stimulation condition was first normalized by its value at 4 ms, and then averaged among multiple cells. To restore absolute values of the S–D curves for each stimulation condition

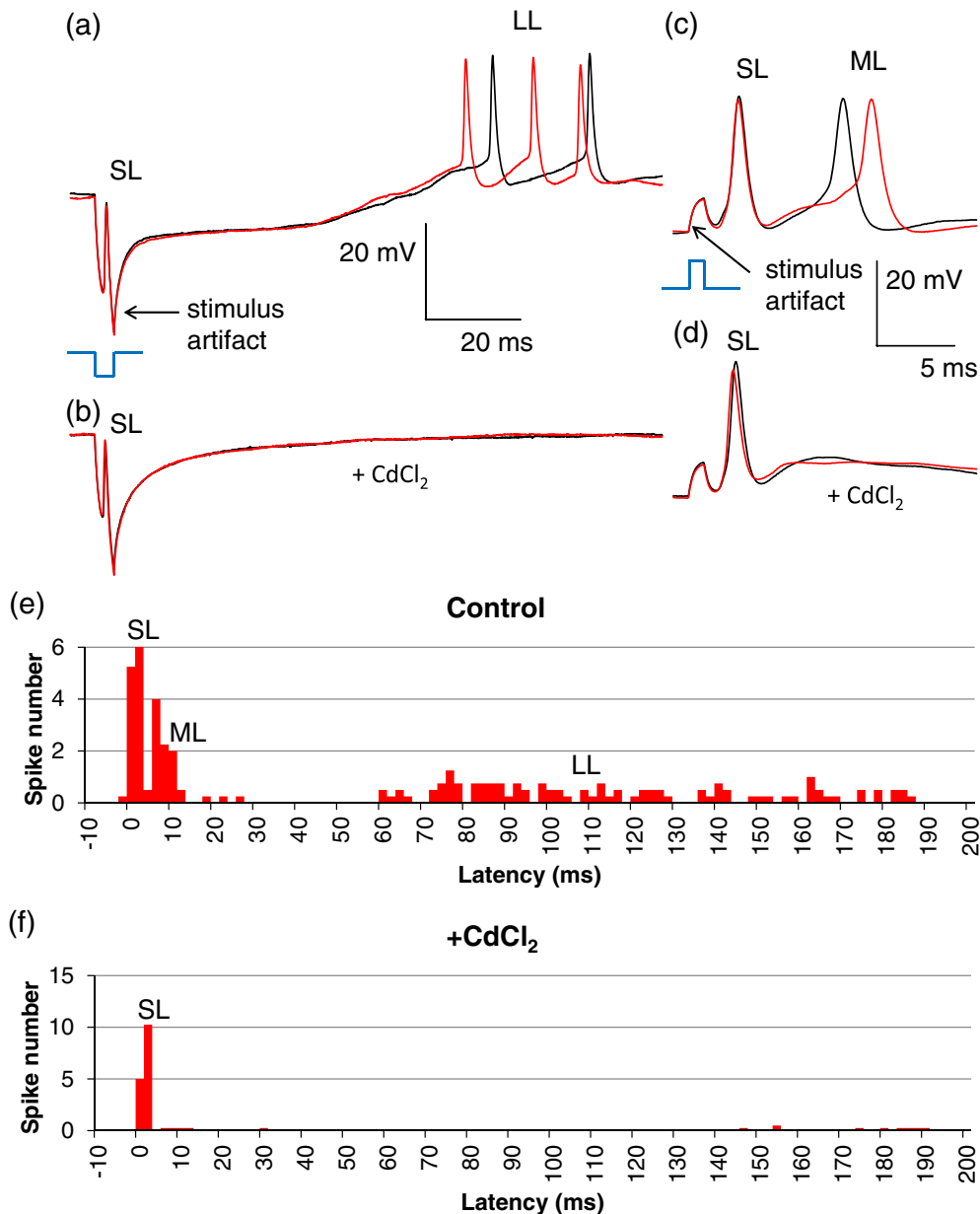


Figure 4. Effect of CdCl_2 on stimulation. (a) The SL and LL responses of RGCs to 4 ms, 25 μA cathodic stimuli applied via subretinal electrode. (b) After addition of CdCl_2 the LL responses disappear, while the SL remain. Stimulus is shown in blue, and scale bars are the same for (a) and (b). (c) SL and ML responses to anodic stimuli of 1 ms, 4 μA applied via electrode in OPL position. (d) After addition of CdCl_2 the ML responses disappear, while the SL remain. Stimulus is shown in blue, and scale bars are the same for (c) and (d). (e) and (f) Disappearance of LL and ML, and preservation of SL response upon addition of CdCl_2 . PSTH represents 4 RGCs with 20 traces per cell.

the geometrical average of the stimulation thresholds at 4 ms was calculated for each response type, pulse polarity and electrode location. Multiplying the normalized S–D curve by the average threshold at 4 ms restores the absolute thresholds for each stimulation condition, as shown in figures 6(a), (b).

Figure 6(a) shows the S–D relationships for epiretinal stimulation with cathodic pulses. The direct stimulation threshold exhibited chronaxy of about 1 ms (in agreement with previous measurements by Jensen *et al* 2005), while the network (ML) threshold continued a constant-slope decrease with increasing pulse duration up to about 10 ms, and started approaching rheobase beyond that duration. Both S–D

relationships were well approximated with the Weiss equation (solid lines in figure 6).

Since the shape of the S–D curves is defined only by the type of stimulation (direct or network) and does not depend on pulse polarity and electrode location, it can be calculated for any other polarity and location by multiplying the epiretinal cathodic curves in figure 6(a) by the ratio of the corresponding thresholds listed in table 1 (available from stacks.iop.org/JNE/11/026008/mmedia). Figure 6(b) shows the S–D relationships for intraretinal (OPL) stimulation with anodic pulses. In this condition, the threshold of the network-mediated response was always lower than that of direct stimulation. LL response became dominant (had lowest

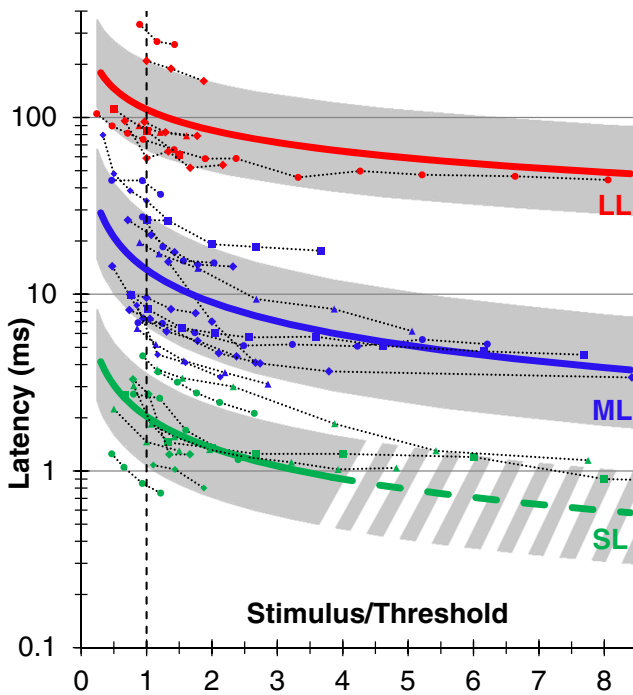


Figure 5. Dependence of the RGC response latency on stimulus strength. Pulse amplitude is expressed as a ratio to stimulation threshold. For each response type, the average is plotted as a solid line, and standard deviation as a shaded area. Traces of individual cells ($N = 30$) with different stimulation thresholds, pulse durations and electrode locations are shown with dash lines.

threshold) at pulse durations exceeding 20 ms, and it continued a constant-slope decline with increasing pulse duration, at least up to 100 ms.

Selectivity of epi-, sub- and intraretinal stimulation

To elicit a specific type of response from RGC while avoiding another effect, the threshold of the desired effect should be lower than that of the undesired one. The span of stimuli strength between these thresholds (undesired to desired) represents the dynamic range for selective stimulation. Figure 6(c) depicts the ratio of the network and direct stimulation thresholds from the figure 6(a), illustrating how the direct selectivity increases with decreasing pulse duration for epiretinal cathodic stimuli.

Average stimulation thresholds for epiretinal ($N = 8$) and IPL ($N = 11$) positions with cathodic and anodic pulses of 0.5 ms in duration are shown in figure 7(a) and in table 1. For example, the threshold for direct response to epiretinal cathodic pulse was $2.4 \mu\text{A}$, and for the network $7.2 \mu\text{A}$, corresponding to direct selectivity of 3. Insertion of the electrode into IPL increased cathodic thresholds at 0.5 ms for both, the direct and network responses: to 5.3 and $8.2 \mu\text{A}$, respectively, but decreased anodic thresholds: from 10 and $21 \mu\text{A}$ to 7.6 and $14 \mu\text{A}$, respectively. Cathodic stimulus in epiretinal position had the highest direct selectivity at pulse durations of 0.5 ms and shorter (figure 6(c) and table 1).

Average stimulation thresholds for IPL ($N = 11$), OPL ($N = 23$) and subretinal ($N = 20$) positions with cathodic and anodic pulses of 4 ms are shown in figure 7(b) and in

table 1. In subretinal placement, anodic pulses had lower thresholds (2.9 and $4.0 \mu\text{A}$ for the network and direct responses at 4 ms) than cathodic (25 and $23 \mu\text{A}$), and the thresholds of the INL-mediated response (ML) to anodic pulses were lower than the direct (SL) ones. Upon electrode insertion into the OPL, the thresholds for both polarities decreased, and network selectivity improved: the direct threshold with anodic polarity became more than twice higher than that of the network with 4 ms pulses (figure 7 and table 1). OPL anodic stimulation provided the lowest threshold and the highest network selectivity among the six different configurations. Figure 6(d) depicts the ratio of the direct and network stimulation thresholds from the figure 6(b), illustrating how the network selectivity increases with increasing pulse duration for OPL anodic stimuli.

Discussion

Disappearance of the ML and LL responses and preservation of the SL spiking upon addition of a universal synaptic blocker— CdCl_2 demonstrated that ML and LL stimulation is mediated by the retinal network, while SL response results from the direct activation of RGCs.

The dominant effect of L-AP4 is the transmission blocking from photoreceptors to ON-bipolar cells by metabotropic (mGluR6) receptor blockade (Pin and Duvoisin 1995), and therefore disappearance of the LL response to electrical stimulation upon addition of L-AP4 is likely to indicate its origin in the photoreceptors. Additional evidence to that conclusion is based on the fact that stimulation thresholds of the LL responses become the lowest among retinal neurons at durations exceeding 20 ms (figure 6(b)). This is in agreement with results from Freeman *et al* (2010), demonstrating that photoreceptors had the lowest thresholds among retinal neurons stimulated by sinusoidal waveforms at low frequencies. However, a possibility that LL responses arise from the lateral spread of the electrical stimulation via horizontal and amacrine cells cannot be excluded, since it also might be affected by the L-AP4 blocker, either directly or via ON bipolar cells.

Lack of the L-AP4 blocker effect on ML response in ON RGCs reveals that this type of stimulation originates in the INL (bipolar, horizontal or amacrine cells). These conclusions are also in accordance with the fact that direct response latency is the shortest—not exceeding 5 ms, while the INL-mediated responses take 3–70 ms, and photoreceptor-mediated bursting begins after 40 ms. In some borderline cases, with latencies in the range of 3–5 or 40–70 ms, addition of the corresponding neurotransmitter blockers is required for accurate classification of the responses.

In earlier stages of retinal degeneration the photoreceptors lose their outer segments, leading to blindness, but their nuclei are preserved to large extent (Buskamp *et al* 2010). Therefore, not only ML but also LL responses could be expected in degenerate retinas, although stimulation thresholds might be affected by the disease. These assumptions remain to be tested in the future experiments with retinas at various stages of degeneration.

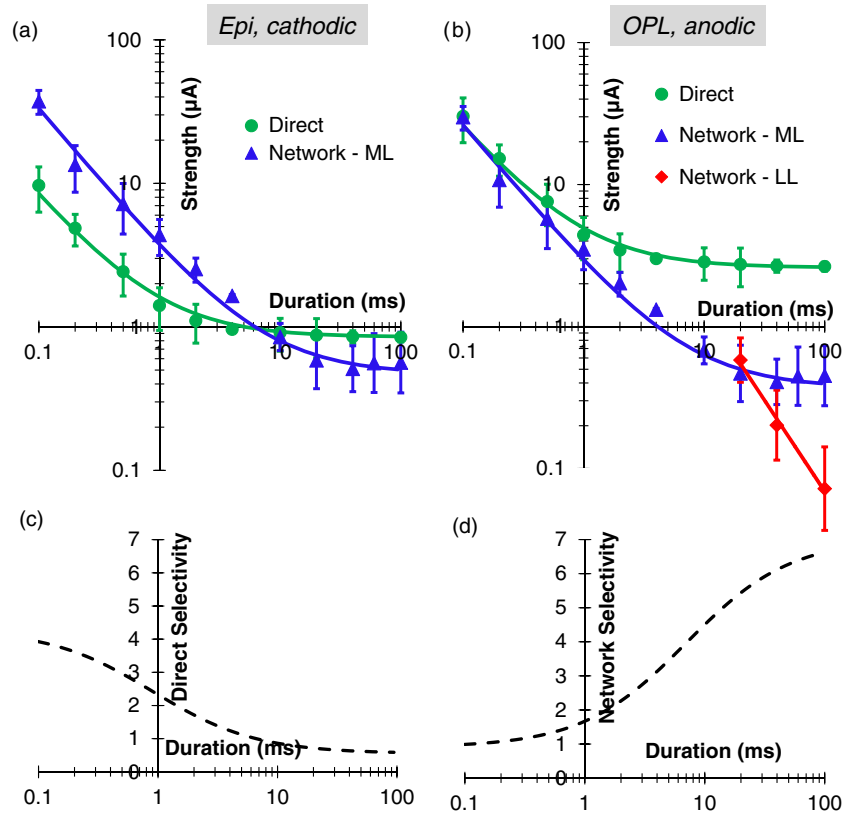


Figure 6. Strength—duration (S–D) relationships of the network-mediated and direct responses. (a) Epiretinal cathodic stimuli. Direct response curve was fitted with Weiss equation $I = 0.85(1 + 0.9/\tau)$, and the network with $I = 0.47(1 + 7/\tau)$. (b) S–D curves for OPL electrode and anodic pulse. Direct curve (SL) was fitted with $I = 2.6(1 + 0.9/\tau)$, ML with $I = 0.37(1 + 7/\tau)$, LL with $I = 26\tau^{-1.3}$. (c) Selectivity for direct response to epiretinal cathodic pulse. (d) Selectivity of the network response to anodic pulse applied via electrode in OPL.

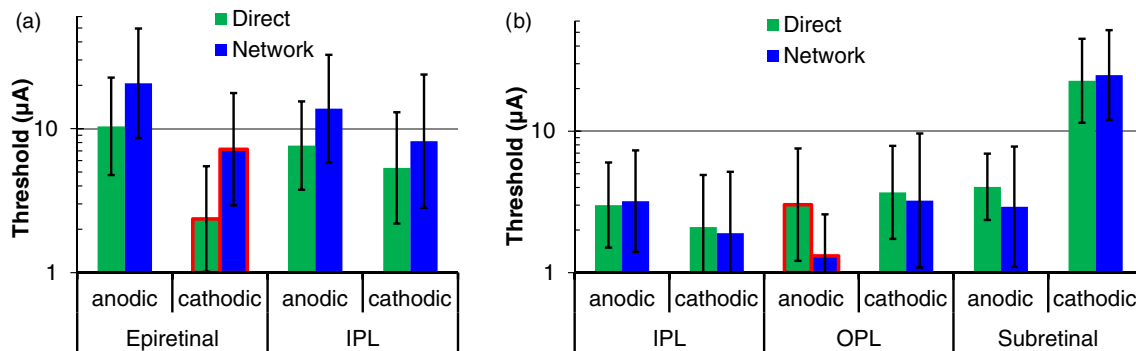


Figure 7. Thresholds of the direct and network-mediated (ML) responses with anodic and cathodic stimuli and electrodes located in epiretinal, IPL, OPL and subretinal positions. (a) Targeting direct stimulation of RGCs: epiretinal and IPL thresholds for 0.5 ms pulses. Optimum configuration for direct stimulation—epiretinal cathodic—is outlined with red. (b) Targeting network-mediated stimulation: IPL, OPL and subretinal thresholds for 4 ms pulses. Optimum configuration for network stimulation – OPL anodic – is outlined with red.

Similarly to the retinal and cortical responses to pulsed light (Levick 1973, Bolz *et al* 1982, Connolly and Gruzeliy 1982), latency of the RGC responses to electrical stimuli decreased with increasing stimulus strength, for all three types of responses (figure 5). Latencies of the network-mediated stimulation were much closer to those of the natural light-induced response than direct stimulation.

This study confirmed that cathodic pulses delivered via epiretinal electrodes are optimal for direct stimulation of RGCs (Jensen *et al* 2005): they have the lowest thresholds,

and direct selectivity is highest at pulse durations below 0.5 ms. These properties of epiretinal stimulation have been already utilized in commercial epiretinal system ARGUS II (da Cruz *et al* 2013). In practice, however, placement of the electrode array in close and stable proximity to epiretinal surface turned out to be very challenging. Clinical results demonstrated that electrodes of the ARGUS II array were found at distances ranging from 0 to 400 μm from the retina, and stimulation thresholds increased with distance (Ahuja *et al* 2013).

To stabilize the array and ensure close proximity to the target neurons, shallow insertion of the needle electrodes into the retina was proposed (Ganesan *et al* 2010, Gefen 2012). Positioning of the electrodes inside IPL, however, increased the direct stimulation threshold and decreased direct selectivity by approximately a factor of 2, which might still be a better arrangement than much higher (up to a factor of 10) thresholds with electrodes floating far above the retina (Ahuja *et al* 2013). Another potential benefit of the intraretinal placement is a possibility of avoiding axonal stimulation—one of the problems of the epiretinal prostheses resulting in arcuate visual perception (Nanduri *et al* 2012). Since our patch-clamp recordings did not discriminate between the somatic and axonal stimulation of RGCs, this conjecture remains to be explored in the future.

On average, threshold of the direct epiretinal stimulation of RGCs with cathodic pulses was significantly lower than with anodic ($p = 0.003$). This can be explained by much higher density of sodium ion-channels in axonal hillocks of RGCs than in other parts of the cell soma (Fried *et al* 2009). Cathodic pulse applied via epiretinal electrode depolarizes the proximal part of the cell soma, including axonal hillock, resulting in reduced stimulation threshold compared to anodic pulse, which hyperpolarizes the proximal part of the cell (Boinagrov *et al* 2012). Therefore, positioning the electrode below the RGC, in the IPL, decreases the anodic threshold and increases the cathodic threshold, compared to the epiretinal position. Higher density of ion-channels (activated at depolarization) at the axons of bipolar cells can similarly explain the lower cathodic than anodic thresholds for network response in epiretinal and IPL positions. For the same reasons in OPL and in subretinal position, the anodic pulses have lower thresholds than cathodic for the direct and network (ML) responses (see figure 7 and supplementary table 1).

Network-mediated approach to retinal stimulation, generating a burst of ML spikes in response to a single stimulus, is best implemented with electrode placement in the outer retina, i.e. below the INL. Inside the OPL, anodic pulses have the lowest thresholds ($1.3 \mu\text{A}$ at 4 ms), and network selectivity increases with pulse duration (figure 6(d)), exceeding a factor of 5 at 20 ms. At pulse durations exceeding 20 ms, the LL response becomes dominant (i.e. has lowest threshold), although it is not clear whether this type of response will be present in degenerate retina (due to lack of photoreceptors). It is also important to keep in mind that photoreceptors above the subretinal implant disappear shortly after chronic implantation due to their separation from the retinal pigmented epithelium, so the OPL becomes the most realistic approximation of the electrodes location *in-vivo*, even with a wild-type retina (Mandel *et al* 2013).

Diameter of subretinal electrode ($40 \mu\text{m}$) was much larger than the pipette used in the other three locations ($4\text{--}8 \mu\text{m}$). However, this should not have any major effect on the stimulation thresholds since the distance to the target neurons—RGCs ($\sim 150 \mu\text{m}$) and INL ($\sim 70 \mu\text{m}$) was several times larger than the radius of subretinal electrode ($r = 20 \mu\text{m}$).

Stimulation thresholds vary from cell-to-cell very significantly, as can be seen from the large error bars in figure 7.

Factors contributing to this strong cell-to-cell variability may include differences in RGC size, morphology of its dendritic tree, as well as the extent of its network and its position relative to the stimulation electrode. Since previous studies of the direct stimulation thresholds (Tsai *et al* 2009, Cho *et al* 2013) have found no significant difference between the stimulation thresholds of ON and OFF RGCs, they have not been separated in the S–D plots in the current study.

The current study utilized monopolar electrodes with large distant return, similar to the subretinal and epiretinal prostheses used in clinical trials (da Cruz *et al* 2013, Stingl *et al* 2013). However, bipolar electrodes with local returns may provide better confinement of electric field, and therefore may result in higher selectivity for both epiretinal and subretinal stimulation.

In clinical practice, the stimulation is performed with biphasic charge-balanced pulses. There is infinite number of ways to construct the second phase (different waveforms, durations, inter-pulse intervals, etc), and different prosthetic systems implement various options. For example, our photovoltaic system (Mathieson *et al* 2012) has a nearly-square first phase, and a much longer exponential second phase with lower amplitude. Stimulation properties of this system are very well approximated by the square monophasic pulses of the current study. In the capacitor-coupled ‘push’ generators the first phase is usually square, but the second phase has exponential falling edge. In the ‘push–pull’ generators both phases can be square, but they can have different durations and delays between them. In this study we characterized the most basic pulse shape—a single phase rectangular waveform.

In conclusion, we demonstrated that epiretinal cathodic stimulation with pulse durations below 0.5 ms is optimal for eliciting direct response of RGCs while avoiding network-mediated spiking, as long as very close proximity to the retinal surface can be assured. Shallow ($\sim 30 \mu\text{m}$) insertion of the thin electrodes into the retina may help stabilize their positioning, but it increases stimulation thresholds and decreases direct selectivity by approximately a factor of 2. For network-mediated stimulation, the optimal position is in the OPL, with anodic pulses of long durations (> 10 ms), providing the lowest threshold and highest network selectivity.

Acknowledgments

We thank Keith Mathieson and Lele Wang for their help with manufacturing the SIROF electrode arrays for subretinal stimulation, Roopa Dalal for retinal histology images. This project was supported by the NIH grant R01EY018608, Stanford University Bio-X Research grant, Air Force Office of Scientific Research grant FA9550-10-1-0503.

Conflict of interest. The authors declare no competing financial interests.

References

- Ahuja A K, Yeoh J, Dorn J D, Caspi A, Wuyyuru V, McMahon M J, Humayun M S, Greenberg R J, daCruz L and Argus II Study Group 2013 Factors affecting perceptual thresholds in Argus II retinal prosthesis subjects *Trans. Vis. Sci. Tech.* **2** 1

- Bendali A, Dubus E, Dégardin J, Lissorgues-Bazin G, Rousseau L, Djilas M, Bergonzo P, Benosman R, Picaud S and Sahel J-A 2012 Retinal prostheses: diamond biocompatibility and 3D structure ARVO'12: Annu. Meeting of the Association for Research in Vision and Ophthalmology paper 5528/D1133
- Boinagrov D, Loudin J and Palanker D 2010 Strength-duration relationship for extracellular neural stimulation: numerical and analytical models *J. Neurophysiol.* **104** 2236–48
- Boinagrov D, Pangratz-Fuehrer S, Suh B, Mathieson K, Naik N and Palanker D 2012 Upper threshold of extracellular neural stimulation *J. Neurophysiol.* **108** 3233–8
- Bolz J, Rosner G and Wässle H 1982 Response latency of brisk-sustained (X) and brisk-transient (Y) cells in the cat retina *J. Physiol.* **328** 171–90 (PMID: 7131312)
- Busskamp V and Roska B 2011 Optogenetic approaches to restoring visual function in retinitis pigmentosa *Curr. Opin. Neurobiol.* **21** 942–6
- Busskamp V et al 2010 Genetic reactivation of cone photoreceptors restores visual responses in retinitis pigmentosa *Science* **329** 413–7
- Butterwick A, Huie P, Jones B W, Marc R E, Marmor M and Palanker D 2009 Effect of shape and coating of a subretinal prosthesis on its integration with the retina *Exp. Eye Res.* **88** 22–29
- Cho A, Sampath A P, Humayun M S and Weiland J D 2013 Physiological response of RD mouse retinal ganglion cells to electrical stimulation ARVO'13: Annu. Meeting of the Association for Research in Vision and Ophthalmology paper 1035/C0012
- Connolly J F and Gruzelić J H 1982 Amplitude and latency changes in the visual evoked potential to different stimulus intensities *Psychophysiology* **19** 599–608
- da Cruz L et al 2013 The Argus II epiretinal prosthesis system allows letter and word reading and long-term function in patients with profound vision loss *Br. J. Ophthalmol.* **97** 632–6
- Daiger S P, Bowne S J and Sullivan L S 2007 Perspective on genes and mutations causing retinitis pigmentosa *Arch. Ophthalmol.* **125** 151–8
- Eickenscheidt M, Jenkner M, Thewes R, Fromherz P and Zeck G 2012 Electrical stimulation of retinal neurons in epiretinal and subretinal configuration using a multicapacitor array *J. Neurophysiol.* **107** 2742–55
- Enzmann V, Yolcu E, Kaplan H J and Ildstad T S 2009 Stem cells as tools in regenerative therapy for retinal degeneration *Arch. Ophthalmol.* **127** 563–71
- Ferris F L III, Fine S L and Hyman L 1984 Age-related macular degeneration and blindness due to neovascular maculopathy *Arch. Ophthalmol.* **102** 1640–2
- Freeman D K, Eddington D K, Rizzo J F and Fried S I 2010 Selective activation of neuronal targets with sinusoidal electric stimulation *J. Neurophys.* **104** 2778–91
- Fried S I, Hsueh H A and Werblin F S 2006 A method for generating precise temporal patterns of retinal spiking using prosthetic stimulation *J. Neurophysiol.* **95** 970–8
- Fried S I, Lasker A C W, Desai N J, Eddington D K and Rizzo J F III 2009 Axonal sodium-channel bands shape the response to electric stimulation in retinal ganglion cells *J. Neurophysiol.* **101** 1972–87
- Fujikado T et al 2011 Testing of semichronically implanted retinal prosthesis by suprachoroidal-transretinal stimulation in patients with retinitis pigmentosa *Invest. Ophthalmol. Vis. Sci.* **52** 4726–33
- Ganesan K, Stacey A, Meffin H, Lichter S, Greferath U, Fletcher E L and Prawer S 2010 Diamond penetrating electrode array for epi-retinal prosthesis *Proc. Annu. Int. Conf. of the IEEE Engineering in Medicine and Biology Society* pp 6757–60
- Gefen R 2012 Nano-retina project status 7th Biennial World Congress on Artificial Vision (Detroit, MI)
- Hadjinicolaou A E et al 2012 Electrical stimulation of retinal ganglion cells with diamond and the development of an all diamond retinal prosthesis *Biomaterials* **33** 5812–20
- Hottowy P, Skoczeń A, Gunning D E, Kachiguine S, Mathieson K, Sher A, Wiacek P, Litke A M and Dąbrowski W 2012 Properties and application of a multichannel integrated circuit for low-artifact, patterned electrical stimulation of neural tissue *J. Neural Eng.* **9** 066005
- Humayun M S et al 2011 Interim results from the international trial of Second Sight's visual prosthesis *Ophthalmology* **119** 779–88
- Jensen R, Ziv O and Rizzo J III 2005 Thresholds for activation of rabbit retinal ganglion cells with relatively large, extracellular microelectrodes *Invest. Ophthalmol. Vis. Sci.* **46** 4
- Jeon C J, Strettoi E and Masland R H 1998 The major cell populations of the mouse retina *J. Neurosci.* **18** 8936–46 (PMID: 9786999)
- Jones B W and Marc R E 2005 Retinal remodeling during retinal degeneration *Exp. Eye Res.* **81** 123–37
- Khraiche M L, Lo Y, Wang D, Cauwenberghs G, Freeman W and Silva G A 2011 Ultra-high photosensitivity silicon nanophotonics for retinal prosthesis: electrical characteristics *Proc. Annu. Int. Conf. of the IEEE Engineering in Medicine and Biology Society* pp 2933–6
- Kim S Y, Sadda S, Pearlman J, Humayun M S, de Juan E Jr, Melia B M and Green W R 2002 Morphometric analysis of the macula in eyes with disciform age-related macular degeneration *Retina* **22** 471–7
- Klauke S, Goertz M, Rein S, Hoehl D, Thomas U, Eckhorn R, Bremmer F and Wachtler T 2011 Stimulation with a wireless intraocular epiretinal implant elicits visual percepts in blind humans *Invest. Ophthalmol. Vis. Sci.* **52** 449–55
- Levick W R 1973 Variation in the response latency of cat retinal ganglion cells *Vis. Res.* **13** 837–53
- Loudin J D, Simanovskii D M, Vijayraghavan K, Sramek C K, Butterwick A F, Huie P, McLean G Y and Palanker D V 2007 Optoelectronic retinal prosthesis: system design and performance *J. Neural Eng.* **4** S72–84
- Mandel Y et al 2013 Cortical responses elicited by photovoltaic subretinal prostheses exhibit similarities to visually evoked potentials *Nature Commun.* **4** 1980
- Margalit E and Thoreson W B 2006 Inner retinal mechanisms engaged by retinal electrical stimulation *Invest. Ophthalmol. Vis. Sci.* **47** 2606–12
- Margolis D J, Gartland A J, Euler T and Detwiler P B 2010 Dendritic calcium signaling in ON and OFF mouse retinal ganglion cells *J. Neurosci.* **30** 7127–38
- Mathieson K et al 2012 Photovoltaic retinal prosthesis with high pixel density *Nature Photon.* **6** 391–7
- Mazzoni F, Novelli E and Strettoi E 2008 Retinal ganglion cells survive and maintain normal dendritic morphology in a mouse model of inherited photoreceptor degeneration *J. Neurosci.* **28** 14282–92
- Nanduri D, Fine I, Horsager A, Boynton G M, Humayun M S, Greenberg R J and Weiland J D 2012 Frequency and amplitude modulation have different effects on the percepts elicited by retinal stimulation *Invest. Ophthalmol. Vis. Sci.* **53** 205–14
- Palanker D, Huie P, Vankov A, Aramant R, Seiler M, Fishman H, Marmor M and Blumenkranz M S 2004 Migration of retinal cells through a perforated membrane: implications for a high-resolution prosthesis *Invest. Ophthalmol. Vis. Sci.* **45** 3266–70
- Palanker D, Vankov A, Huie P and Baccus S 2005 Design of a high-resolution optoelectronic retinal prosthesis *J. Neural Eng.* **2** S105–20

- Phelan J K and Bok D 2000 A brief review of retinitis pigmentosa and the identified retinitis pigmentosa genes *Mol. Vis.* **6** 116–24 www.molvis.org/molvis/v6/a16/
- Pin J P and Duvoisin R 1995 The metabotropic glutamate receptors: structure and functions *Neuropharmacology* **34** 1–26
- Polosukhina A *et al* 2012 Photochemical restoration of visual responses in blind mice *Neuron* **75** 271–82
- Reutsky-Gefen I, Golan L, Farah N, Schejter A, Tsur L, Brosh I and Shoham S 2013 Holographic optogenetic stimulation of patterned neuronal activity for vision restoration *Nature Commun.* **4** 1509
- Rizzo J F III, Wyatt J, Humayun M, de Juan E, Liu W, Chow A, Eckmiller R, Zrenner E, Yagi T and Abrams G 2001 Retinal prosthesis: an encouraging first decade with major challenges ahead *Ophthalmology* **108** 13–14
- Sakmann B and Neher E 1984 Patch clamp techniques for studying ionic channels in excitable membranes *Annu. Rev. Physiol.* **46** 455–72
- Schraermeyer U, Thumann G, Luther T and Kociok N 2001 Subretinally transplanted embryonic stem cells rescue photoreceptor cells from degeneration in the RCS rats *Cell Transplant.* **10** 673–80
- Sekirnjak C, Hottowy P, Sher A, Dabrowski W, Litke A M and Chichilnisky E J 2006 Electrical stimulation of mammalian retinal ganglion cells with multielectrode arrays *J. Neurophysiol.* **95** 3311–27
- Stett A, Barth W, Weiss S, Haemmerle H and Zrenner E 2000 Electrical multisite stimulation of the isolated chicken retina *Vis. Res.* **40** 1785–95
- Stingl K *et al* 2013 Artificial vision with wirelessly powered subretinal electronic implant alpha-IMS *Proc. R. Soc. B* **280** 20130077
- Stone J L, Barlow W E, Humayun M S, de Juan E and Milam A H 1992 Morphometric analysis of macular photoreceptors and ganglion cells in retinas with retinitis pigmentosa *Arch. Ophthalmol.* **110** 1634–9
- Tsai D, Morley J W, Gregg J, Suaning G J and Lovell N H 2009 Direct activation and temporal response properties of rabbit retinal ganglion cells following subretinal stimulation *J. Neurophysiol.* **102** 2982–93
- Weiland J D, Liu W and Humayun M S 2005 Retinal prosthesis *Annu. Rev. Biomed. Eng.* **7** 361–401
- Zrenner E 2002 Will retinal implants restore vision? *Science* **295** 1022–5